Proceedings of the
International Conference on Mechanical Engineering 2005
(ICME2005) 28- 30 December 2005, Dhaka, Bangladesh

ICME05-FL-20

GENERATION OF MICRO DROPLETS USING UNSTEADY EXPANSION WAVE AND ITS CONTROL

Miah Md. Ashraful Alam[1], Shigeru Matsuo[2], Masanori Tanaka[1], Md. Mahbubul Alam[1] and Toshiaki Setoguchi[2]

[1] Graduate School of Science and Technology, Saga University, 1 Honjo-machi, Saga-shi, Saga 840-8502, Japan.
[2] Deptartment of Mechanical Engineering, Saga University, 1 Honjo-machi, Saga-shi, Saga 840-8502, Japan.

ABSTRACT

Aerosol particles are closely related to the field of science, engineering, agriculture and pharmacy, and in order to solve problems of aerosol, it is considered that it is important to investigate the generating method of the particles. In the present study, a computational fluid dynamics work is applied to investigate the generation of micro droplets and possibility of its control using both an unsteady expansion wave propagating upstream of the inlet of an elliptical cell and an unsteady jet flow emitted into the cell. In simulations, the unsteady two dimensional Euler equations and the theory of non-equilibrium condensation of moist air are used to clarify the effect of the geometry of the cell inlet and the duration time of the jet on spatiotemporal distributions of cluster size and flow properties in the elliptical cell.

Keywords: Compressible Flow, Homogeneous Condensation, Elliptical Cell, Unsteady Expansion Wave, Numerical Simulation.

1. INTRODUCTION

Recently, aerosol particles in the atmosphere have attracted interest for environmental pollution and health of human. In hospitals, food and semiconductor industries, these are treated as a toxic substance. However, in chemical process, development and use of a medicine and agricultural chemicals, these have been treated as useful particles. Lately for development of new material using nanoparticles, the manufacturing techniques and usage become the centre of strong interest. As is obvious from these examples, aerosol particles are closely related to the field of science, engineering, agriculture and pharmacy, and in order to solve problems of aerosol, it is important to investigate the generating method of the particles.

Laser ablation cluster source has a long history of use for the generation of cluster beams. The ablated material is cooled by collisions with the carrier gas atoms, and initiates the growth of clusters [1]. Clusters are expanded into vacuum with a wide distribution of cluster sizes through a nozzle. For the topics, there were few researches for the distribution of cluster size in space and the time-dependent growth of clusters. However, recently, it has been reported that an application of focusing phenomenon of the induced shock propagating in the ellipsoidal-shaped cluster cell enable to control the size of a spatiotemporal confined cluster source [2].

When moist air or steam expands rapidly in a nozzle, a non-equilibrium condensation occurs at a supersaturated state rather than at its equilibrium saturated state [3, 4, 5]. Many theoretical and experimental researches were carried out for this phenomenon in a Laval nozzle, and in regard to the supersonic flow, the effects of non-equilibrium condensation on the flow-field have been almost made clear.

In the present study, a computational fluid dynamics work is applied to investigate a generation of micro droplets and possibility of its control using both an unsteady expansion wave propagating upstream of the inlet of an elliptical cell and an unsteady jet flow emitted into the cell. In simulations, the unsteady two dimensional Euler equations and the theory of non-equilibrium condensation of moist air are used to clarify the effect of the geometry of the cell inlet and the duration time of the jet on spatiotemporal distributions of cluster size and flow properties in the elliptical cell.

2. CFD ANALYSIS

2.1 Governing Equations

Assumptions using in the present calculation of the two phase flow are as follows : Both velocity slip and temperature difference do not exist between condensate particles and gas mixture, and the effect of the condensate particles on pressure is neglected. The governing equations are the unsteady two dimensional Euler equations and droplet growth equation [5] written in a Cartesian coordinate system (x,y) as follows;

$$\frac{\partial \boldsymbol{U}}{\partial t}+\frac{\partial \boldsymbol{E}}{\partial x}+\frac{\partial \boldsymbol{F}}{\partial y}=\boldsymbol{Q} \qquad (1)$$

where

$$\boldsymbol{U}=\begin{bmatrix}\rho_m\\ \rho_m u\\ \rho_m v\\ E_s\\ \rho_m g\\ \rho_m D_1\\ \rho_m D_2\\ \rho_m D_3\end{bmatrix},\ \boldsymbol{E}=\begin{bmatrix}\rho_m u\\ \rho_m u^2+p\\ \rho_m uv\\ u(E_s+p)\\ \rho_m ug\\ \rho_m uD_1\\ \rho_m uD_2\\ \rho_m uD_3\end{bmatrix},\ \boldsymbol{F}=\begin{bmatrix}\rho_m v\\ \rho_m uv\\ \rho_m v^2+p\\ v(E_s+p)\\ \rho_m vg\\ \rho_m vD_1\\ \rho_m vD_2\\ \rho_m vD_3\end{bmatrix},\ \boldsymbol{Q}=\begin{bmatrix}0\\ 0\\ 0\\ 0\\ \rho_m \dot{g}\\ \rho_m \dot{D}_1\\ \rho_m \dot{D}_2\\ \rho_m \dot{D}_3\end{bmatrix} \quad (2)$$

where

$$E_s=\rho_m C_{p0}T+\frac{1}{2}\rho_m\left(u^2+v^2\right)-\rho_m gL \quad (3)$$

$$p=G\left[E_s-\frac{1}{2}\rho_m\left(u^2+v^2\right)+\rho_m gL\right] \quad (4)$$

$$G=\left(1-g\frac{M_m}{M_v}\right)\Big/\left(\frac{1}{\gamma-1}+g\frac{M_m}{M_v}\right) \quad (5)$$

Subscripts *m* and *v* refer to mixture and vapor, respectively. *k* is thermal conductivity. The latent heat *L* is given by a function of temperature [6] ;

$$L(T)=L_0+L_1T \ \text{J/kg} \quad (6)$$
$$L_0=3105913.39\ \text{J/kg},\quad L_1=-2212.97\ \text{J/kg}$$

The condensate mass fraction *g* is given by a rate equation, expressed by Eq.(7) [5].

$$\dot{g}=\frac{dg}{dt}=\frac{\rho_l}{\rho_m}\left(\frac{4\pi}{3}{r_c}^3 I+\rho_m D_1\frac{dr}{dt}\right) \quad (7)$$

In Eq.(2), $\dot{D}_1$, $\dot{D}_2$, and $\dot{D}_3$ are given as:

$$\dot{D}_1=\frac{dD_1}{dt}=\frac{4\pi\,{r_c}^2 I}{\rho_m}+D_2\frac{dr}{dt} \quad (8)$$

$$\dot{D}_2=\frac{dD_2}{dt}=\frac{8\pi\,r_c I}{\rho_m}+D_3\frac{dr}{dt} \quad (9)$$

$$\dot{D}_3=\frac{dD_3}{dt}=\frac{8\pi I}{\rho_m} \quad (10)$$

Nucleation rate *I*, critical radius of the nuclei r_c and radius growth rate $\dot{r}$ are given as follows [5][6] :

$$I=\frac{1}{\rho_l}\left(\frac{2m_v\sigma}{\pi}\right)^{1/2}\left(\frac{p_v}{\kappa T}\right)\exp\left(\frac{-4\pi\,r_c\sigma}{3T\kappa}\right) \quad (11)$$

$$r_c=\frac{2\sigma}{\rho_l\Re_v T\ln\left(p_v/p_{s,\infty}\right)} \quad (12)$$

$$\dot{r}=\frac{dr}{dt}=\frac{1}{\rho_l}\frac{p_v-p_{s,r}}{\left(2\pi\Re_v T\right)^{1/2}} \quad (13)$$

In the above equations, *m*, κ, $\Re$ and $p_{s,\infty}$ are the molecular weight, Boltzmann constant, the gas constant and the flat film equilibrium vapor pressure, respectively. The density of liquid phase is given by a function of temperature [6] ;

$$\left.\begin{aligned}\rho_l(T)&=\frac{A_0+A_1t+A_2t^2+A_3t^3+A_4t^4+A_5t^5}{1+B_0t}\\ &\quad \text{kg/m}^3,\ (t\ge 0\ ^\circ\text{C})\\ \rho_l(T)&=A_6+A_7t+A_8t^2\ \text{kg/m}^3,\ (t<0\ ^\circ\text{C})\end{aligned}\right\} \quad (14)$$

where *t* is the temperature given by °C and the coefficients are given by :

$$A_0=999.8396,\ A_1=18.224944,$$
$$A_2=-7.92221\times10^{-3},\ A_3=-55.44846\times10^{-6},$$
$$A_4=149.7562\times10^{-9},\ A_5=-393.2952\times10^{-12},$$
$$A_6=999.84,\ A_7=0.086,\ A_8=-0.0108,$$
$$B_0=18.159725\times10^{-3}$$

The surface tension $\sigma(=\sigma_\infty)$ [6], that is an infinite flat-film surface, is given by ;

$$\left.\begin{aligned}\sigma_\infty(T)&=\{76.1+0.155(273.15-T)\}\times10^{-3},\\ &\quad \text{for } T\ge 249.39\ \text{K}\\ \sigma_\infty(T)&=\{(1.1313-3.7091\times10^{-3}\times T)\\ &\quad \times T^4\times10^{-4}-5.6464\}\times10^{-6},\\ &\quad \text{for } T<249.39\ \text{K}\end{aligned}\right\} \quad (15)$$

In Eq.(14), $p_{s,\infty}$ is also given as [6] :

$$p_{s,\infty}(T)=\exp\left(A_9+A_{10}T+A_{11}T^2+B_1\ln(T)+\frac{C_0}{T}\right)\ \text{N/m}^3 \quad (16)$$
$$A_9=21.125,\ A_{10}=-2.7246\times10^{-2},$$
$$A_{11}=1.6853\times10^{-5},\ B_1=2.4576,\ C_0=-6094.4642$$

where *T* is the temperature given by K. Using flat film equilibrium vapor pressure $p_{s,\infty}$ above, the saturation vapor pressure $p_{s,r}$ of condensate droplet with a radius of *r* in Eq.(13) is given by Thompson-Gibbs equation [5] ;

$$p_{s,r}=p_{s,\infty}\exp\left(\frac{2\sigma_\infty}{\rho_l\Re_v Tr}\right) \quad (17)$$

The governing equation systems that are non-dimensionalized with reference values at the inlet conditions upstream of the nozzle, are mapped from the physical plane into a computational plane of a general transform. A third-order TVD (Total Variation Diminishing) finite difference scheme with MUSCL approach [7] is used to discretize the spatial derivatives, and a second-order fractional step is employed for time integration.

The validity of the method used in the present calculation is shown in the previous research [8].

2.2 Computational Conditions

Figures 1(a) and 1(b) show details of elliptical cell with a straight tube (Type A) and a converging nozzle (Type B) upstream of the inlet, respectively. The lengths of major and minor axes of the elliptical cell are 26.0 mm and 16.0 mm, respectively. The heights of inlet are D =1.0 mm and 4.0 mm. The height of elliptical cell exit is set at D_e= 2.0 mm.

A diaphragm is located at the cell inlet with an origin (x=0), and separates the high pressure side from low-pressure one. After the rupture of diaphragm, the working gas that is moist air, is issued from the cell inlet. The pressure ratio which means the ratio of the reservoir pressure p_0 (atmospheric pressure) and back pressure p_b, is denoted by φ(= p_0/ p_b). In the present study, value of φ is set at 4.0.Value of the initial degree of supersaturation S_0 (= $p_{v0}/p_{s,\infty}$) is 0.6 for both cases. Total temperature T_0 and total pressure p_0 in the reservoir are 298.15 K and 101.3 kPa, respectively.

The number of grids is 35×40 in the region upstream of the cell inlet, and in the region of the cell, it is 530×135 for Fig.1(a) and 400×135 for Fig.1(b). Inlet and exit boundaries are constrained with free boundary condition. The slip-wall, iso-pressure and no heat transfer are constrained on the solid wall. Furthermore, in order to investigate the effect of the duration time of jet on the flow field, the jet issued from the cell inlet was stopped after t_s = 20 and 50 μs from the diaphragm rupture.

3. RESULTS AND DISCUSSION

Figures 2 and 3 show contour maps of static pressure p and condensate mass fraction g in the elliptical cell for Types A (D = 4 mm, t = 11.41 ~ 414.0 μs) and B (D = 4 mm, t = 14.40 ~ 393.6 μs), respectively. Figures 2(d) and 3(d) correspond to contour maps at the time that the liquid phase along the center-line of the elliptical cell reaches at the exit of the cell. In Figs.2 and 3, a shock wave propagates into the cell after the rupture of diaphragm and reaches the exit of cell. A reflected shock wave interacts with the flow issued from the nozzle. As a result, the interaction leads to a very complicated wave structure.

As seen from Fig.2, the non-equilibrium condensation occurs in the jet issuing from the inlet after the diaphragm rupture. The liquid phase spreads spatially with time and propagates to the exit of the cell. Furthermore, the condensate occurs in an unsteady expansion wave even in upstream range of the cell inlet. As a result, it is considered that the occurrence of condensate has an effect on spatiotemporal size of droplets in the cell.

In Fig.3, spatiotemporal distributions of static pressure and condensate mass fraction are very complicated in the same manner as those in Fig.2. However, the condensate occurs

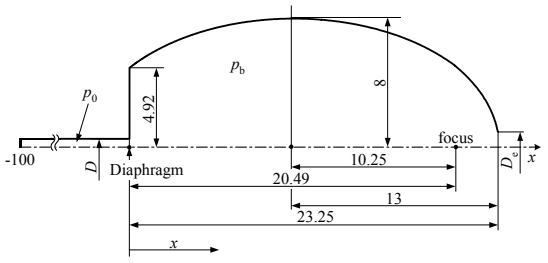

(a) Type A

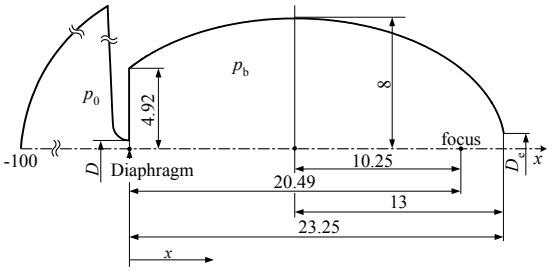

(b) Type B

Fig 1. Details of elliptical cell (Unit : mm)

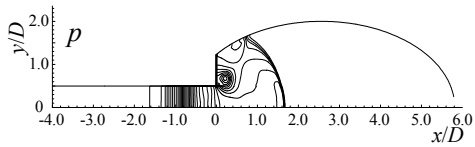

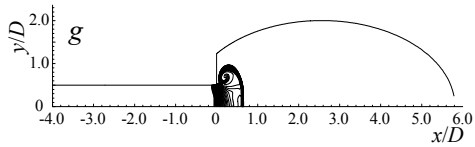

(a) t = 14.40 [μs]

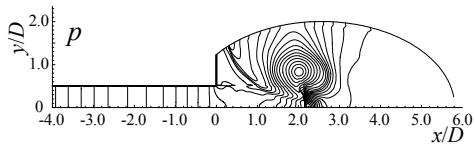

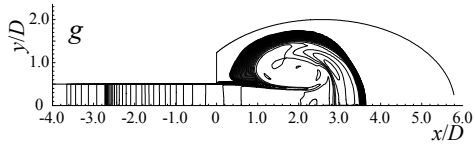

(b) t = 113.5 [μs]

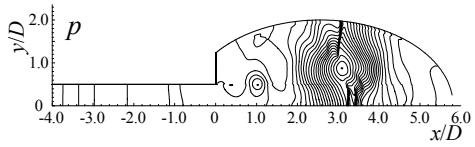

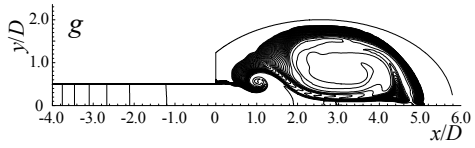

(c) t = 217.5 [μs]

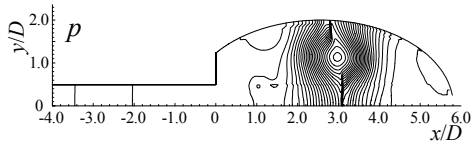

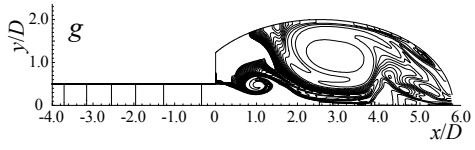

(d) t = 393.6 [μs]

Fig 2. Contour maps of static pressure and condensate mass fraction (Type A, D = 4 mm)

only in the cell and this is different from the result of Fig.2.

Figures 4 and 5 show contour maps of static pressure and condensate mass fraction for the free jet in cases of Types A (D = 4 mm, t = 13.18~418.1 μs) and B (D = 4 mm, t = 14.12 and 245.2 μs), respectively. In Fig.4, the liquid phase spreads over the surrounding space with time and large vortices are observed in the flow field. In Fig.5, the occurrence of the liquid phase is similar to that due to the condensation in the supersonic jet [8]. As seen from these figures, spatiotemporal distributions for p and g are quite different from those in the flow field in cases with the elliptical cell.

In the present study, it is very important to clarify the time-dependent flow properties and growth of cluster at the cell exit in order to examine how the size of a spatiotemporal confined cluster source is controlled.

Figures 6(a) and 6(b) show the time histories of average droplet radius $\bar{r}$ at the cell exit (x=23.25 mm) for D = 1.0 mm and 4.0 mm in cases of Types A and B, respectively. Time history in case of free jet flow at the same position is also shown for reference (D = 4.0 mm). Horizontal axis in Fig.6 indicates the elapsed time after the diaphragm rupture.

In both figures, the average droplet radius $\bar{r}$ in case of D = 1 mm changes largely with time compared with the case of D = 4 mm. Furthermore, $\bar{r}$ for Type A is larger compared with the case of Type B. It is considered that this is due to the growth of droplets generated in upstream range of the cell inlet. In each figure, $\bar{r}$ for D =1.0 mm and 4.0 mm is almost the same after the steep increase. For the free jet, $\bar{r}$ for Type A changes remarkably with time compared with the case of Type B.

Figures 7(a) and 7(b) show time histories of particle number density $\bar{n}$ at the cell exit (x=23.25 mm) for D = 1.0 mm and 4.0 mm in cases of Types A and B, respectively. Time history in case of free jet flow is shown in the same manner as that in Fig.4. In both figures, $\bar{n}$ for the free jet is large compared with that of the elliptical cell, and a large number of droplets are obtained for Type B compared with the case of Type A.

As seen from these results, the geometry of the cell inlet has strong effect on the droplet size and number density, and the suitable cell for capture of many droplets with small radius is the elliptical one with the converging nozzle (Type B).

Figures 8(a) and 8(b) show the effect of the duration time t_s of the jet on time histories of average droplet radius $\bar{r}$ and particle number density $\bar{n}$ at the cell exit in the elliptical cell, respectively. Time histories in case of free jet flow at the same position for Types A and B are also shown for reference (D = 4.0 mm). In Fig.8(a), the average droplet radius in t_s = 20 and 50 μs for Types A and B becomes small compared with that for constant jet flows. Furthermore, it becomes almost constant for Type B after t = 400 μs. In Fig.8(b), particle number densities reach the maximum for t_s = 20 μs. It is found that the duration time of the jet is important to obtain many particles with small radius.

4. CONCLUSIONS

In the present study, a computational fluid dynamics work is applied to investigate a generation of micro droplets and possibility of its control using both an unsteady expansion wave propagating upstream of the inlet of an elliptical cell and an unsteady jet flow emitted into the cell. As a result, it was found that the flow and condensate properties in the cell for high pressure ratio were affected strongly by the height of cell exit. The results obtained shows that wave structures in the elliptical cell became very complicated compared with those for free jet. The occurrence of condensate in upstream range of the cell inlet (Type A) had an effect on spatiotemporal size of droplet in the cell.

The geometry of the cell inlet has strong effect on the droplet size and number density, and the suitable cell for capture of many droplets with small radius is the elliptical one with the converging nozzle (Type B).

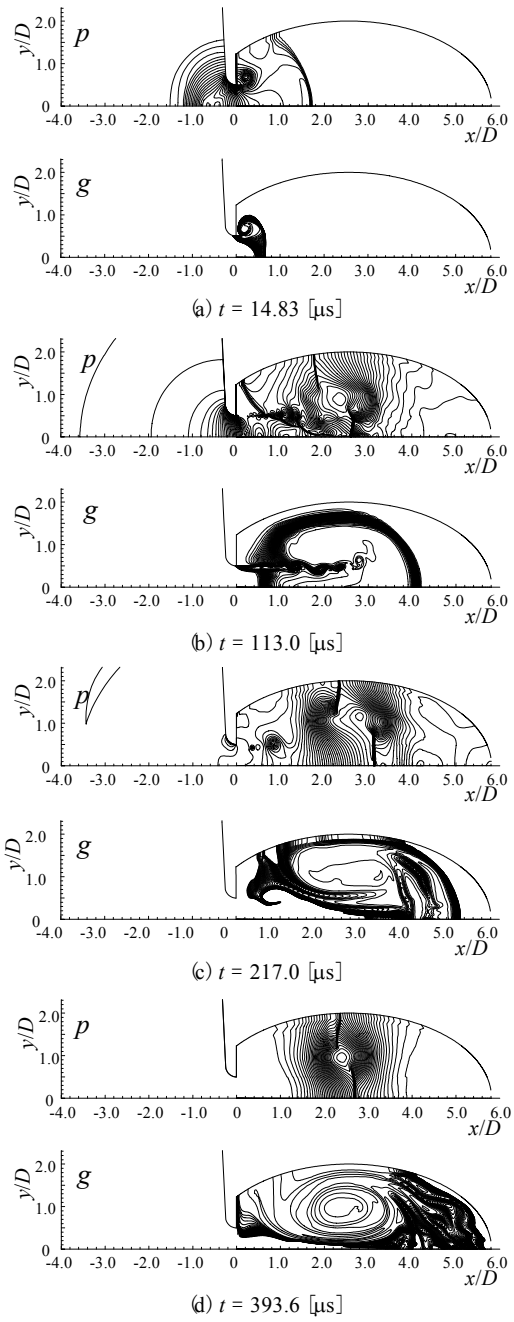

Fig 3. Contour maps of static pressure and condensate mass fraction (Type B, D = 4 mm)

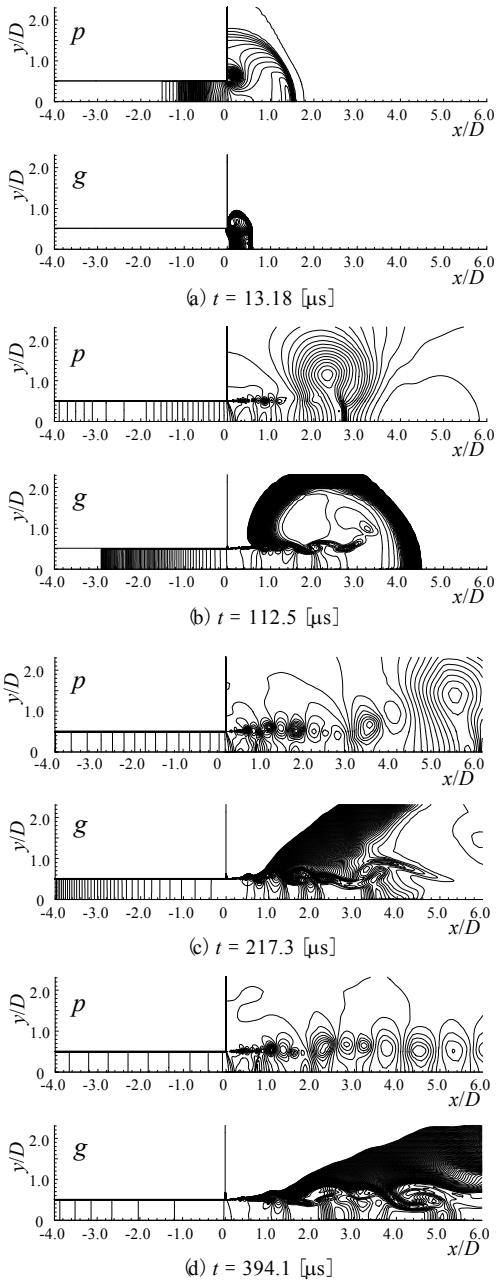

Fig 4. Contour maps of static pressure and condensate mass fraction (Type A, Free jet, D = 4 mm)

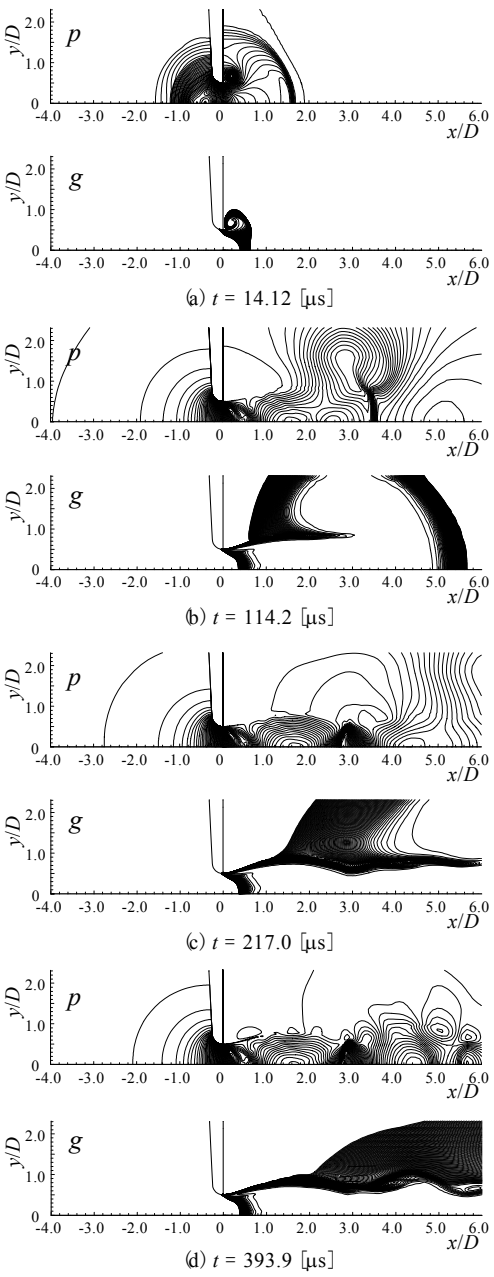

Fig 5. Contour maps of static pressure and condensate mass fraction (Type B, Free jet, D = 4 mm)

5. REFERENCES

1. Han, M., Kiyama, S., Muto, M., Fukuda, A., Sawada, T. and Iwata, Y., 1999, "Cluster formation dynamics in a locally-confined gas layer mixed with the plume ablated by pulsed laser irradiation", Nuclear Instruments and Methods in Physics Research B 153, pp. 302-308.
2. Iwata, Y., Kishida, M.,Muto, M., Yu S., Sawada T., Fukuda, A., Takiya, T., Komura, A. and Nakajima, K., 2002, "Narrow size-distributed silicon cluster beam generated using a spatiotemporal confined cluster source", Chemical Physics Letters 358, pp. 36-42.
3. Hill, P.G., 1966, "Condensation of Water Vapour during Supersonic Expansion in Nozzle", Journal of Fluid Mech. 25 part 3, pp. 593-620.
4. Wegener, P.P. and Wu, B., 1977, "Nucleation Phenomena, Gasdynamics and Homogeneous Nucleation", ed. by Zettlemoyer, A. C., pp. 325-402.
5. Sislian, J. P., 1975, "Condensation of water vapour with or without a carrier gas in a shock tube", UTIAS Report 201.
6. Adam, S., 1999, "Numerische und Experimentelle Untersuchung Instationärer Düsenströmungen mit Energiezufuhr durch Homogene Kondensation", Dissertation, Fukaltät für Maschinenbau, Universität Karlsruhe (TH), Germany.
7. Yee, H.C., 1989, "A class of high-resolution explicit and implicit shock capturing methods", NASA TM-89464.
8. Matsuo, S., Tanaka, M., Setoguchi, T., and Kim, H.D., 2003, "A Study of Under-expanded Supersonic Moist Air Jet", *Proc. of the 17th Symposium on Computational Fluid Dynamics, CD-ROM, (2003)*

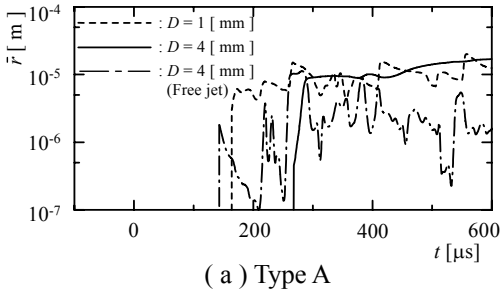

(a) Type A

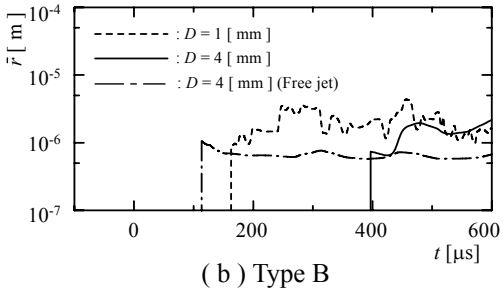

(b) Type B

Fig 6. Time histories of average droplet radius at cell exit

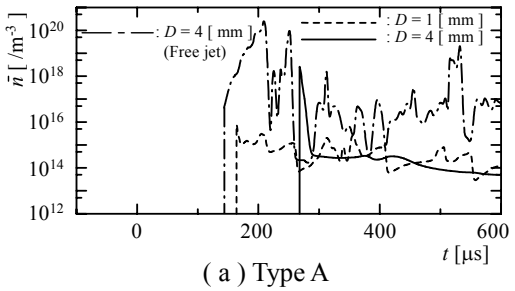

(a) Type A

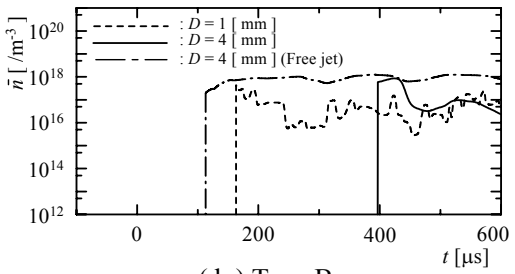

(b) Type B

Fig 7. Time histories of particle number density at cell exit

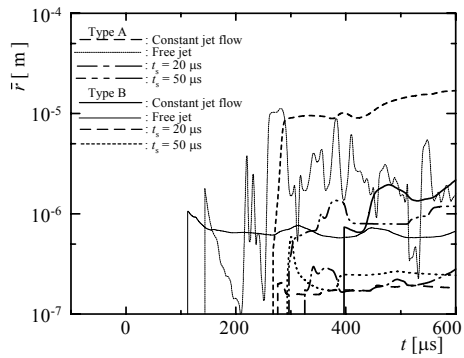

(a) Average droplet radius

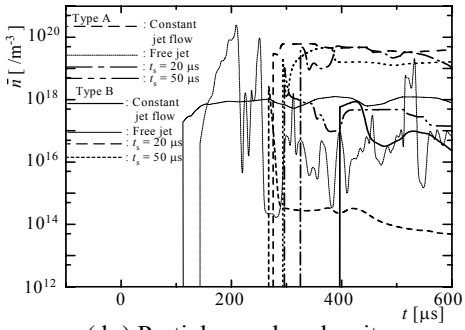

(b) Particle number density

Fig 8. Time histories of average droplet radius and particle number density at cell exit (D = 4 mm)

6. NOMENCLATURE

Symbol	Meaning	Unit
c_p	Specific heat at constant Pressure	(J/kg·K)
D	Diameter	(m)
$\boldsymbol{E},\boldsymbol{F}$	Inviscid flux term	(-)
E_s	Total energy per unit volume	(J/m^3)
g	Condensate mass fraction	(-)
I	Nucleation rate per unit time and volume	(1/s·m^3)
k	Boltzmann constant	(J/K)
L	Latent heat	(J/kg)
M	Molecular weight	(kg/kmol)
M_e	Mach number at the cell exit	(-)
$\bar{n}$	Average particle number density	(m^{-3})
p	Static pressure	(Pa)
$p_{s,r}$	Saturation vapour pressure of condensate droplet with radius of r	(Pa)
$p_{s,\infty}$	Flat film equilibrium vapour pressure	(Pa)
$\boldsymbol{Q}$	Source term of condensation	(-)
r	Radius	(m)
$\bar{r}$	Average droplet radius	(m)
r_c	Critical radius	(m)
$\Re$	Gas constant	(J/kg·K)
S	Degree of supersaturation	(-)
t	Time, Temperature	(s, ºC)
T	Temperature	(K)
u, v	Velocity components	(m/s)
$\boldsymbol{U}$	Conservative vector	(-)
x, y	Cartesian coordinates	(m)
Symbols		
γ	Ratio of specific heat	(-)
φ	Pressure ratio	(-)
ρ	Density	(kg/m^3)
σ	Surface tension	(N/m)
ω	vorticity ($\lvert \partial u/\partial y - \partial v/\partial x \rvert$)	(s^{-1})
Subscripts		
0	Stagnation	
a	Air	
l	Liquid	
m	Mixture	
s	Saturation	